ACS Sustainable Chemistry & Engineering

Research Article

pubs.acs.org/journal/ascecg

# PVA/Gluten Hybrid Nanofibers for Removal of Nanoparticles from Water

Brahatheeswaran Dhandayuthapani, Ramakrishna Mallampati, Deepa Sriramulu, Roshan Fredrick Dsouza, and Suresh Valiyaveettil*

Materials Research Laboratory, Department of Chemistry, National University of Singapore, 3 Science Drive 3, Singapore 117543

Supporting Information

**ABSTRACT:** Recent developments in nanotechnology led to the incorporation of many nanomaterials into consumer products. Disposal of such products will lead to potential contamination of the environment. Nanomaterials are emerging contaminants in water and show significant toxicity to living systems. Considering the diversity in structure and properties, removal of nanopollutants from water warrants novel methods and materials. The objective of this study was to prepare PVA/gluten hybrid nanofibers, which are nontoxic and biodegradable adsorbents for the extraction of nanopollutants from water. Surface morphology, elemental composition, and functional groups on the fiber surface were established using microscopic and spectroscopic techniques. Influence of analytical factors such as experimental pH, time, and concentration of the pollutants toward establishing the efficiency of extraction were quantified using UV−vis spectroscopy. Nanofiber mats with 5 wt % gluten exhibited high extraction efficiency of 99% toward citrate-capped silver (Ag) and gold (Au) nanoparticles with a maximum adsorptive capacity of 31.84 mg/g for Ag NPs and 36.54 mg/g for AuNPs. The kinetic and equilibrium adsorption data were interpreted using Freundlich and Langmuir isotherm models, and a potential adsorption mechanism was suggested. The adsorption kinetics showed a pseudo-second-order model for the extraction of nanoparticles. The prepared PVA/gluten hybrid nanofibers can be utilized as an efficient low-cost adsorbents for removal and recovery of metal nanoparticles from the aqueous environment.


**KEYWORDS:** *PVA, Gluten, Nanofiber, Nanoparticle, Environmental*

## INTRODUCTION

Scarcity of drinking water is becoming a critical global issue owing to an increase in environmental pollution. The contaminants in untreated natural water include suspended particulates such as clay, silt, fine particles of natural organic matter, inorganic matter, plankton, and microscopic organisms. Recently, a few classes of nanomaterials, such as functional nanomaterials (e.g., carbon nanotubes and metal nanoparticles), have generated environmental concerns, especially when such materials are manufactured and used on a large scale in consumer products, which usually end up in the environment through uncontrolled disposal.[1] Industrial nanowastes have greater diversity of particles and may include colloidal metal oxides, silica, metal particles, dispersed polymers, and dyes. Nanomaterials are considered emerging pollutants, and toxicities of such materials in living organisms have been studied by several research groups.[2] For example, carbon nanotubes are toxic and can induce granulomas in animal lungs.[3,4] Metal and metal oxide nanoparticles induce inflammatory and toxic responses in living systems.[5,6] Because of rapid population growth, mismanagement of water resources, and increasing population, the development of new and efficient adsorbents for water purification is necessary to prevent harmful nanoparticles entering into the potable water supply.

The nanofibers or nanostructured fiber mats prepared using the electrospinning technique are used for tissue engineering,[7−9] optical sensors,[10] catalysts,[11−13] protective clothing,[14] ultrafiltration,[15] and separation processes.[16−19] Because of their high specific surface area, large number of surface functional groups, and stability, electrospun nanofibers are expected to be a good adsorbent for pollutants via physical or chemical adsorption. Recently, thiol and amine functionalized PVA nanofiber mats were used successfully for the adsorption of nanoparticles from water.[20−23] Gluten is particularly interesting as a raw material for the development of new biomaterials for environmental application owing to their low cost and easy accessibility.[24,25] A widely used approach is to consider the gluten system as a polymer network that is stabilized by various interactions, such as covalent bonds, noncovalent interactions (hydrogen bonds and hydrophobic interactions), and entanglements.[26] Therefore, developing nanofibers from natural

Received: January 1, 2014
Revised: February 5, 2014
Published: February 12, 2014

  

proteins will provide a green substitute for synthetic polymer fibers.

Preparation and characterization of hybrid nanofibers from synthetic polymer, PVA, and gluten for environmental applications is interesting owing to their low toxicity, biodegradability, and mechanical properties.[27−29] In this study, PVA/gluten hybrid nanofiber mats were fabricated and used as adsorbents. Incorporation of gluten in the fiber is expected to increase the number and type of functional groups on the surface for enhancing the interaction with pollutants. Analytical factors such as extraction time, concentration of pollutants, and pH were explored to obtain optimum extraction efficiency. We hypothesize that hybrid PVA/gluten nanofibers could be useful for the removal of dissolved pollutants from water.

## EXPERIMENTAL DETAILS

**Materials.** Polyvinyl alcohol (PVA, $M_w$ = 146,000−186,000), wheat gluten (crude, ≥ 80% protein), silver nitrate ($AgNO_3$), hydrogen tetrachloroaurate trihydrate ($HAuCl_4{\cdot}H_2O$), sodium citrate tribasic dihydrate ($Na_3C_6H_5O_7{\cdot}2H_2O$), and sodium borohydride ($NaBH_4$) were purchased from Sigma Aldrich and used as received. Glutaraldehyde was purchased from Merck. The solvents used were of analytical grade and purchased from local suppliers. Ultrapure water was used for preparation of solutions.

**Synthesis of Citrate-Capped Gold and Silver Nanoparticles.** Citrate-capped gold nanoparticles (Au NPs) were synthesized following a reported procedure.[30] Aqueous solution of $HAuCl_4{\cdot}3H_2O$ ($5 \times 10^{-3}$ M, 10 mL) was diluted to 190 mL with ultrapure water. Sodium citrate solution (0.5%, 10 mL) and sodium borohydride (0.03 g) were added under constant stirring until a color change to wine red was observed, indicating the formation of a Au NP colloidal solution. The final solution was topped up to 200 mL with water. Similarly, citrate-capped Ag NPs were synthesized by diluting a stock solution of $AgNO_3$ solution ($5 \times 10^{-3}$ M, 25 mL) with 200 mL of water followed by addition of 10 mL of 1% sodium citrate solution (10 mL) and reduction with $NaBH_4$ (0.03 g). Stirring was continued until a color change to pale yellow was observed, and then it was diluted to 250 mL for further use.

**Preparation of PVA/Gluten Solutions for Electrospinning.** The spinning solutions were prepared from a single solvent system. Initially, the PVA (7 wt %) solution was prepared by dissolving PVA powder in distilled water at about 90 °C with constant stirring for 3 h. After the solution was cooled to room temperature, aqueous solution of gluten (2.5 mL and 5 wt %) was added to PVA solutions and stirred for 15 h to acquire a homogeneous solution. Adding higher amounts of gluten showed a phase separation inside the PVA mixture and was not considered in this preliminary examination.

**Fabrication of PVA/Gluten Hybrid Nanofibers by Electrospinning.** For electrospinning, 10 mL of PVA/gluten solution was taken in a 10 mL hypodermic syringe and injected using a syringe pump (Optrobio Technologies Pte, Ltd.) through a blunt-ended needle with an internal diameter of 1.2 mm. The syringe was then attached to a syringe pump operating at a flow rate of 15 $\mu$L min$^{-1}$. The needle was connected to a high voltage supply (ES30P-20W/DDPM/220, Gamma High Voltage, Inc., U.S.A.). An electric field of 1.5 kVcm$^{-1}$ (expressed in terms of voltage/distance) between the collection plate (cathode) and the needle tip (anode) was applied. The collector plate was covered with aluminum foil, and the plate was positioned at a distance of 15 cm from the needle to collect the electrospun fibers. All electrospinning processes were performed at ambient temperature.

**Cross-Linking of Hybrid PVA/Gluten Nanofibers.** Nanofiber mats, chemical cross-linking agent glutalraldehyde (GA, 50%), and trifluoroacetic acid as a catalyst were placed inside a desiccator. Hybrid fiber mats were then allowed to cross-link in the vapor-rich environment for a period of 6 h under ambient condition and stored in air-tight containers in presence of a desiccant until further testing was performed. This method allows the cross-linking to take place on the surface of the fiber. To study the stability of the cross-linked fibers in water, the fiber mats were submerged in deionized water at room temperature for 24 h and then dried overnight for the removal of trace amounts of water before their surface morphology and structural properties were analyzed.

**Sample Characterization.** The Au and Ag NPs were observed under a JEOL 3010 high resolution transmission electron microscope (HRTEM). For sample preparation, a dilute solution of Au NPs or Ag NPs dispersed in ultrapure water was placed onto a carbon-coated copper grid (400 mesh) supported on a clean filter paper, dried overnight, and used for TEM. Dynamic light scattering (DLS) and zeta potential measurements were done using a Malvern Zetasizer Nano-ZS.

The surface morphology and diameter of the fiber samples were analyzed by a JEOL JSM-6701F field emission scanning electron micrograph equipped with an energy dispersive X-ray spectrometer (EDS). The sample was sputter coated with a thin platinum layer using an auto sputter fine coater (JFC 1600, JEOL, Japan) before imaging.

Infrared (IR) spectra of the composite fibers were recorded using a Bruker ALPHA FTIR spectrometer in transmittance mode at room temperature. FTIR spectrum of PVA, gluten, and PVA/gluten blends were acquired using a KBr pellet, and all samples were scanned from the 4000 to 400 cm$^{-1}$ region.

The adsorption measurements of Au NPs and Ag NPs solutions before and after extractions were performed using a UV−vis spectrophotometer (Shimadzu UV-1601PC) at room temperature. The residual amount of nanoparticles after extraction was determined by withdrawing samples at fixed time intervals, recording an absorption spectrum, and calculating the concentration using a calibration curve prepared from standard solution. The intensities at the maximum absorption ($\lambda_{max}$) of the nanoparticle solution were used for the calculation.

## SORPTION STUDIES

**Effect of Contact Time and Concentration on Adsorption Process.** Adsorption studies were carried out using a NPs solution (3 mL) at a concentration range of 2−40 mg L$^{-1}$ for Au NPs and 2−70 mg L$^{-1}$ for Ag NPs with 0.5 g of PVA and PVA/gluten nanofibers. The experiments were carried out at constant initial concentration. The absorbance of the supernatant solution was measured at different time intervals using a spectrophotometer and analyzed for residual nanoparticle concentrations. All adsorption experiments were done at 30 °C using an orbital shaker at 200 rpm. The pollutant adsorbed on the adsorbent at equilibrium $q_e$ (mg/g) was calculated using the following equation,[31]

$$q_e = \left(C_0 - C_e\right)V/M$$

where $C_0$ and $C_e$ (mg/L) are the concentrations of pollutant at initial stage and at equilibrium conditions, respectivey, $V$ (L) is volume of the pollutant solution, and $M$ (g) is mass of the adsorbent used.

**Effect of pH on Adsorption Process.** The effects of pH on nanoparticle adsorption were investigated using 3 mL of initial concentration of Au NP and Ag NP solutions and 0.5 g of nanofiber. The initial pH in the range 1−12 was adjusted using 0.1 M HCl or 0.1 M NaOH. The equilibrium was reached at 80 min for both Au and Ag solutions at ambient conditions. The amount of NPs adsorbed were determined, and the percentage removal of pollutant was calculated as

$$\text{Removal\%} = \left(\frac{C_i - C_f}{C_i}\right)100$$

where $C_i$ and $C_f$ (mg $L^{-1}$) are the initial and final concentration of nanoparticles in water, respectively.

## ADSORPTION KINETICS AND MECHANISM

**Adsorption Isotherm.** Adsorption isotherms, also known as equilibrium data, are the fundamental requirements for the design of adsorption systems. To simulate the adsorption isotherm, two commonly used models, the Freundlich[32] and Langmuir[33] isotherm, were selected to understand the nanoparticle−nanofiber interactions.

**Adsorption Kinetics.** Kinetic models elucidating the mechanism by which pollutants are adsorbed on adsorbent surfaces have been proposed. Adsorption is a time-dependent process, and it is important to know the rate of adsorption for designing and evaluating the adsorbent for the extraction of nanoparticles from water. In many cases, the kinetics of adsorption based on the overall adsorption rate by the adsorbent is described by the pseudo-first-order and pseudo-second-order models.[34−36]

## RESULTS AND DISCUSSION

**Morphology and Structure of Au NPs and Ag NPs.** Figure S1of the Supporting Information shows the TEM images of sodium citrate-stabilized Ag and Au nanoparticles. The Ag NPs and Au NPs showed an average diameter of 25 ± 3 and 35 ± 2 nm, respectively, with a narrow size distribution. The best conditions for getting nonagglomerated nanoparticles were almost spherical and homogeneously dispersed. Sodium citrate acted as the capping agent for these nanoparticles. The particle size distributions for the micrographs are shown in Figure S2 of the Supporting Information.

**Particle Size and Zeta Potential.** The size of the nanoparticles in the solution was established using the dynamic light scattering (DLS) method. Size distributions for the Ag NPs and Au NPs stock solution are given in Figure S3 of the Supporting Information. The histogram of Ag NPs and Au NPs shows particle size ranges from 10 to 70 nm. The average diameters were 25 ± 1.05 and 35 ± 1.19 nm, respectively. High negative zeta potentials of −23 mV (Au NPs) and −25 mV (Ag NPs) were obtained from the DLS studies (Figure S3, Supporting Information).

**Optical Property of Au NPs and Ag NPs.** The UV−vis spectra confirmed the formation of gold and silver nanoparticles. A well-defined surface plasmon band with a broad absorption at about 521 nm (Figure S4, Supporting Information) in the spectrum confirms the existence of Au NPs in the solution. The absorption peak at 387 nm indicates the formation of Ag NPs.[21]

**Fiber Morphology and Diameter.** Mixtures of PVA (7 wt %) and two different concentrations (2.5 and 5 wt %) of gluten were used to prepare the nanofibers. Using optimum electrospinning conditions of applied voltage (15 kV), flow rate (15 $\mu$L $min^{-1}$), and collection distance (15 cm), smooth and uniform nanofibers were obtained.

Figure 1 shows the SEM micrographs of the electrospun PVA and PVA/gluten nanofibrous mats. The diameter and morphology of the fibers were uniform along the fiber axis. The mean diameter of the PVA nanofibers (220 nm) was smaller than that of PVA/gluten nanofibers, which were 285 (2.5 wt %) and 290 nm (5 wt %). All electrospun fibers showed smooth morphology and high stability.

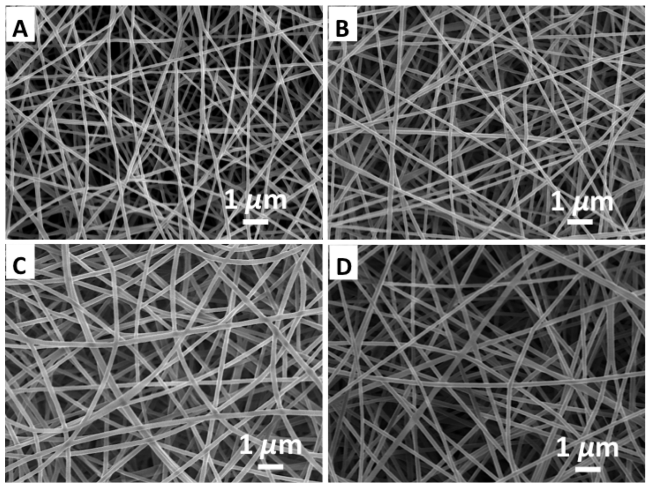


**Figure 1.** SEM micrographs of the electrospun, but not cross-linked PVA fiber (A), PVA cross-linked fiber (B), cross-linked PVA/gluten (2.5 wt %) (C), and PVA/gluten (5 wt %) fibers (D). Electrospining parameters: voltage, 15 kV; flow rate, 15 $\mu$L $min^{-1}$; and collector distance, 15 cm.

**Formation of Water Stable PVA/Gluten Nanofibers.** Chemical cross-linking by glutaraldehyde (GA), which reacts with the hydroxyl groups of the PVA in presence of an acid catalyst, has been well studied.[37,38] The cross-linking process makes the nanofibrous mats water-insoluble and suitable for applications in aqueous medium. Also, the cross-linking process did not change the morphology or diameter of the fibers. Figure 1(B−D) shows the SEM images of the cross-linked water stable fibers. After immersion in water for 48 h, the smooth surface morphologies were well preserved, indicating no leaching or dissolution of the fibers.

After extraction, the presence of the nanoparticles on the surface of the nanofiber was observed using an electron microscope. Figure 2 shows the SEM image of PVA/gluten (5 wt %) after the extraction of Au NPs and Ag NPs on the surface of the nanofiber. The white dots on the fiber surface with high electron density represent the nanoparticles. From the micrographs, the nanoparticles were adsorbed and distributed uniformly on the nanofiber surface without agglomeration or aggregation. Similarly, EDS spectra of the samples show the presence of Au and Ag metal atoms on the surface of the nanofibers (Figure 2C and D).

Figure 3 shows the FTIR spectra of gluten, PVA, and PVA/gluten fibers. Pure PVA showed absorbance peaks for the hydroxyl (−OH) group at 3315 $cm^{-1}$ and a peak corresponding to the −C−O−C group at 1097 $cm^{-1}$. The spectra of the wheat glutens with polypeptide chains showed a strong amide I (C═O) peak at 1650 $cm^{-1}$ and amide II (NH) peak at 1540 $cm^{-1}$, as well as the broad −NH peak in the region of 3100−3500 $cm^{-1}$, which is typical of proteins.[39] The peak at 1540 $cm^{-1}$ of gluten did not shift in the spectrum of the PVA/gluten hybrid fiber, suggesting that gluten may be in a dispersed state within the PVA fiber.

**Effect of Extraction Time on Adsorption Kinetics.** Figure 4A and B show the amount of nanoparticles adsorbed by nanofibers as a function of time. The hybrid nanofibers extract nanoparticles from water more efficiently than pure PVA fibers. Also, the amount of gluten added influenced the extraction efficiency. Hence, a higher initial concentration of nanoparticles will enhance the adsorption process. The graphs indicate a high

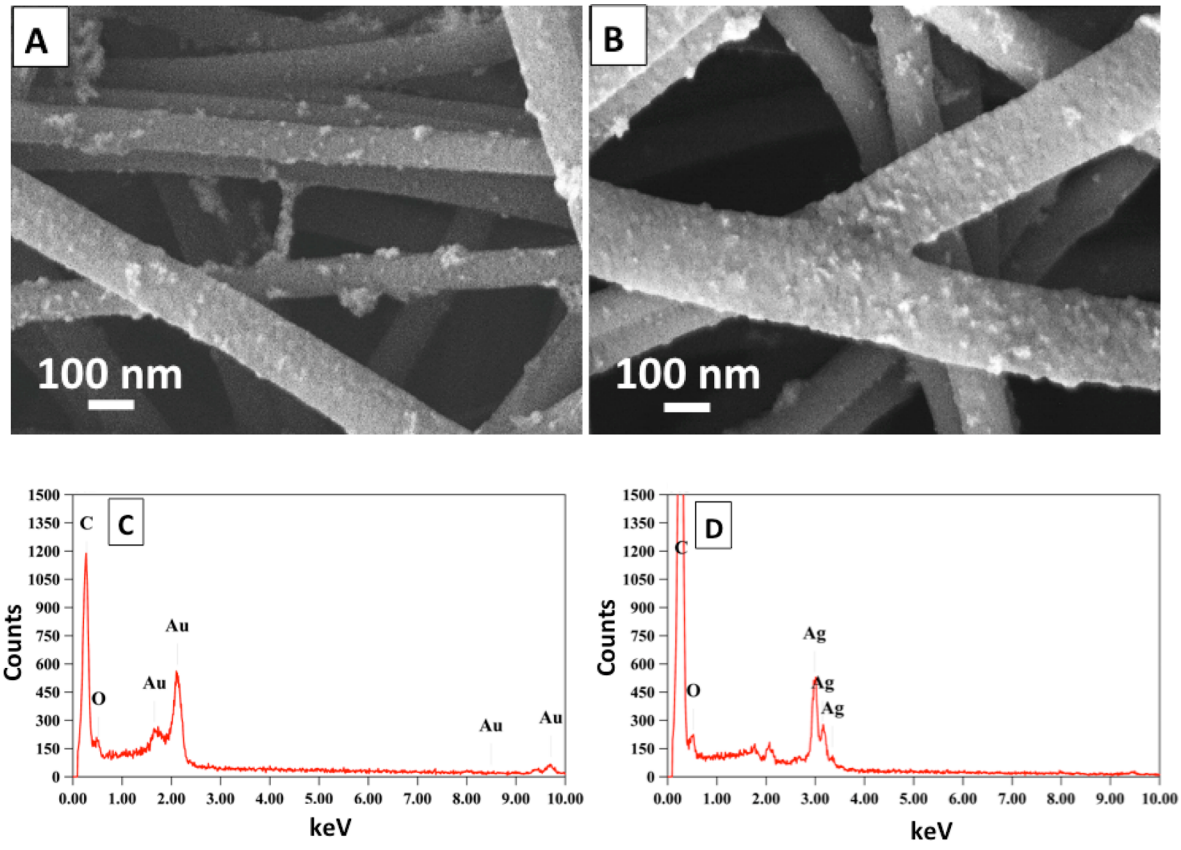


**Figure 2.** SEM image of PVA/gluten (5 wt %) after the extraction of (A) Au NPs and (B) Ag NPs on the surface of the nanofiber and the EDS spectra of the (A) Au and (B) Ag on the fiber surface.

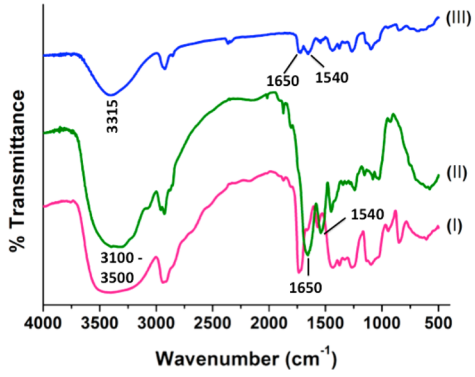


**Figure 3.** FTIR spectra of PVA (I), gluten (II), and PVA/gluten nanofibers (III); peaks confirms the gluten major functional groups of amide 1 (C═O stretching, N−H vibration) at ∼1650 $cm^{-1}$ and amide 2 (NH bending and CN stretching) at ∼1540 $cm^{-1}$, respectively.

adsorption rate during the first hour, and equilibrium was reached within 90 min. When equilibrium was reached, approximately 83% and 99% of Au and Ag NPs were removed by the hybrid nanofiber mats, respectively. It is shown that the adsorption is rapid until equilibrium is reached. The highest adsorption rate was found for the PVA/gluten (5 wt %), and the lowest rate was found for PVA nanofiber. The results clearly indicate that the efficiency of nanoparticle removal increased up to 99% with 5% gluten concentration in the hybrid nanofiber.

The effect of the initial Au NPs and Ag NPs concentrations on the extraction rate by PVA and PVA/gluten nanofibers at a mixing speed of 200 rpm is shown in Figure 5. When concentrations of 40 mg/L (Au NP) and 70 mg/L (Ag NP) were used, extraction capacities of 36 mg/g (Au NP) and 31 mg/g (Ag NP) were observed. PVA nanofibers showed less adsorption capacity for both Ag NPs and Au NPs. The extraction capacity was increased with an increase in the gluten concentration in the nanofiber, which may be attributed to an increase in the number and types of surface functional groups (i.e., −OH, −NHCO−, and $-NH_2$) and hydrophilic nature of the adsorbent. Higher adsorption efficiency of PVA/gluten hybrid nanofibers toward NPs can be attributed to the presence of amide (I and II) groups on the fiber surface. This can be described by the nanoparticle−nanofiber interaction that depends on the functional group present on the nanofiber surface.

**Effect of pH on Adsorption Process.** The effect of pH on the NP extraction efficiency of PVA and PVA/gluten nanofibers was studied at different pH ranging from 4−9 (Figure 6). Both PVA and gluten have a significant number of functional groups such as −OH, $-NH_2$, and −CO−NH− and are known to facilitate hydrogen bonding at neutral pH. Giles and Hassan[40] demonstrated that the polar functional groups on the fiber surface are strongly hydrated and capable of forming hydrogen bonds with anion pollutant.

The maximum percentage removal of Au NPs and Ag NPs occurred at neutral pH, and extraction decreases at acidic and alkaline pH. The percentage of nanoparticle extracted was 92% for PVA/gluten (5 wt %), 80% for PVA/gluten (2.5 wt %), and 42% for PVA nanofibers when the NP solution pH was 7.0, and it decreased to 52%, 38%, and 21%, when the pH of the nanoparticle solution was increased to 9. NPs have a negative surface charge throughout the pH range from 2 to 9.[41] In acidic medium, the surface of the adsorbent is positively charged due

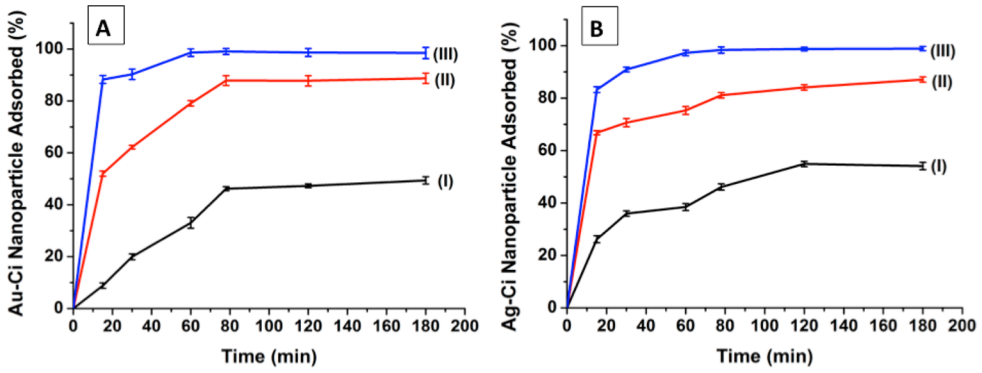


**Figure 4.** Effect of time and amount of (A) Au NPs and (B) Ag NPs adsorbed by (1) PVA fiber, (II) PVA/gluten (2.5 wt %) fiber, and (III) PVA/gluten (5 wt %) nanofiber mats. Initial concentrations of 40 mg $L^{-1}$ for Au NPs and 70 mg $L^{-1}$ for Ag NPs (3 mL) with 0.5 g of PVA. PVA/gluten nanofibers were analyzed.

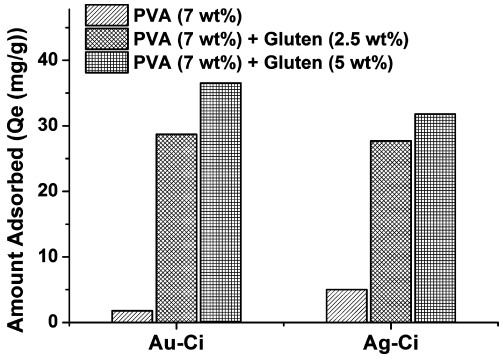


**Figure 5.** Amount of nanoparticles adsorbed and adsorption capacity of the hybrid nanofibers. Initial concentrations of 40 mg $L^{-1}$ for Au NPs and 70 mg $L^{-1}$ for Ag NPs (3 mL) with 0.5 g of PVA. PVA/gluten nanofibers were analyzed.

to the higher concentration of $H^+$ ions; thus, the electrostatic attraction between the nanofiber and negatively charged nanoparticle is enhanced. However, in alkaline conditions, electrostatic repulsion between the negatively charged adsorbent and adsorbate reduces the interaction.

## ■ ADSORPTION ISOTHERMS

**Langmuir Isotherm.** In this study, Langmuir and Freundlich isotherm models were used to describe the basic equilibrium.

The data obtained from the adsorption experiment for different nanoparticles were analyzed using an isotherm equation. The saturation monolayer can be expressed by the equation

$$\frac{1}{q_e} = \frac{1}{q_m} + \frac{1}{Kq_mC_e}$$

$$q_e = \frac{Kq_mC_e}{1 + q_mC_e}$$

The Langmuir constants, $q_m$ (maximum adsorption capacity) (mg/g) and $K_a$ (values for Langmuir constant related to the energy of adsorption (L/mg)) are predicted from the plot between $C_e/q_e$ versus $C_e$.

The effect of the isotherm shape has been discussed with a view to predicting whether an adsorption system is favorable or not favorable. Hall et al.[42] proposed a dimensionless separation

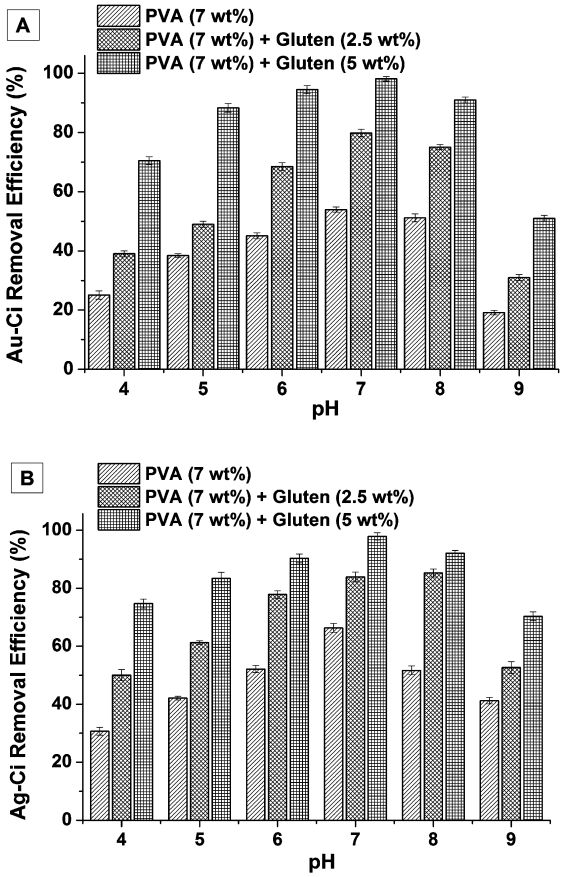


**Figure 6.** Effect of pH on the (A) Au NPs and (B) Ag NPs removal efficiency of PVA and PVA/gluten nanofibers. Initial concentrations of 40 mg $L^{-1}$ for Au NPs and 70 mg $L^{-1}$ for Ag NPs (3 mL) at different pH with 0.5 g of PVA. PVA/gluten nanofibers were analyzed.

factor, $R_L$, as an essential feature of the Langmuir isotherm, which is defined as

$$R_L = \frac{1}{1 + KC_e}$$

where $K$ is the Langmuir constant, and $C_e$ is the initial concentration of the adsorbate in solution.

Figure 7 shows the Langmuir plot for the extraction of Au NPs and Ag NPs. The values of $Q_e$ and $R_L$ are calculated from the slopes and intercepts of the linear plots of $1/Q_e$ vs $1/C_e$


dx.doi.org/10.1021/sc500003k | ACS Sustainable Chem. Eng. 2014, 2, 1014−1021

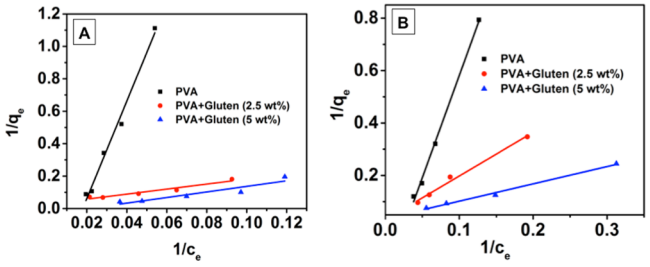


**Figure 7.** Langmuir plot for (A) Au NPs and (B) Ag NPs. Isotherm model plots for the adsorption of nanoparticle concentration range of 2−40 mg $L^{-1}$ for Au NPs and 2−70 mg $L^{-1}$ for Ag NPs (3 mL) with 0.5 g of PVA. PVA/gluten nanofibers were analyzed.

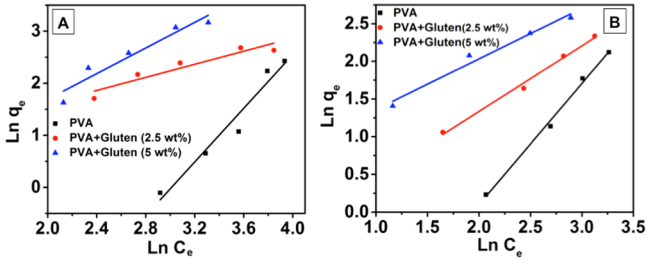


**Figure 8.** Freundlich plot for Au NPs (A) and Ag NPs (B). Isotherm model plots for the adsorption of nanoparticle concentration range of 2−40 mg $L^{-1}$ for Au NPs and 2−70 mg $L^{-1}$ for Ag NPs (3 mL) with 0.5 g of PVA. PVA/gluten nanofibers were analyzed.

(Table 1). The maximum adsorption capacity $Q_e$ is calculated to be 36.54 mg/g for Au NPs and 31.84 mg/g for Ag NPs using our hybrid nanofibers. The data indicates the Langmuir model is more appropriate to explain the nature of adsorption of negatively charged nanoparticles on the fiber surface with correlation coefficients of 0.934 to 0.991 for Au NPs and 0.978 to 0.995 for Ag NPs.

**Freundlich Isotherm.** Figure 8 shows the Freundlich plot for Au NPs and Ag NPs. The Freundlich isotherm is an empirical equation derived to model the multilayer adsorption for heterogeneous surfaces and can be expressed as

$$\ln q_e = \ln K_f + \frac{1}{n} \ln C_e$$

where $q_e$ is the amount of nanoparticle adsorbed per unit of adsorbent at equilibrium time (mg $g^{-1}$), and $C_e$ is equilibrium concentration of NPs in solution (mg $L^{-1}$). $K_f$ and $n$ are isotherm constants that indicate the capacity and intensity of the adsorption, respectively.[43]

The pseudo-second-order equation is based on the adsorption equilibrium capacity and may be expressed in the form

$$\frac{t}{q_t} = \frac{1}{K_2 q_e^{\,2}} + \left(\frac{1}{q_e}\right) t$$

where $k_2$ is the rate constant of the pseudo-second-order adsorption, and $q_e$ is the equilibrium adsorption capacity (mg/g). The $k_2$ and $q_e$ values of different pollutants can be calculated experimentally from the slope, and the intercept of $t/q_t$ versus $t$ plots.

The values of $K_f$ and $1/n$ are calculated using the intercept and slope of the linear plot log $q_e$ vs log $c_e$, and the results are presented in Table 2. The value of $1/n$ is <1 for Au NPs and Ag NPs, which indicates that the adsorption of negatively charged particles on the PVA/gluten hybrid nanofibers is favorable. The overall results show that the PVA/gluten hybrid nanofibers act as an effective and low-cost sorbent for the removal of nanopollutants from aqueous solutions.

**Adsorption Kinetics.** Investigation of adsorption kinetics provides information about the mechanism of adsorption and is important for the validation of the efficiency of the process. In the present work, the kinetic data obtained from batch studies have been analyzed by using pseudo-first-order and pseudo-second-order models.

The integral form of the pseudo-first-order model is generally expressed as

$$\log(q_e - q_t) = \log q_e - \left(\frac{k_1}{2.303}\right) t$$

where $q_e$ and $q_t$ represent the amount of nanoparticles adsorbed (mg/g) at any time $t$ and at equilibrium time, respectively, and $k_1$ represents the adsorption first-order rate constant ($min^{-1}$), and $t$ is the contact time (min). The adsorption rate constant $K_1$ were calculated from the plot of log($q_e - q_t$) against $t$.

Table 3 shows the rate constant, calculated $Q_e$, and regression coefficient of the first-order kinetic model. On the basis of the regression coefficient ($R^2 < 0.89$), it appeared that the first-order model was not an appropriate fit with the experimental data. In addition, the $Q_e$ from the calculation was different from the experimental $Q_e$.

The pseudo-second-order kinetics and rate constants for the extractions were obtained from the pseudo-second-order kinetic model. The extraction data showed a good fit with the pseudo-second-order kinetic model. The regression coefficients of the second-order model ($R^2$ value in the range of 0.97−0.99) were greater than that of the first-order model for both nanoparticles. The results also showed similar experimental and calculated values of $Q_e$. The first- and second-order kinetics model plots are shown in Figures S5 and S6 of the Supporting Information, respectively.

## CONCLUSION

In summary, the influence of two different concentrations of gluten protein on the morphology and properties of electro-

**Table 1. Langumir Isotherm Model Constants and Correlation Coefficients for Adsorption of Two Different Nanoparticles**

| | samples | slope ($1/K_{qm}$) | intercept ($1/q_m$) | $K$ | $R_L$ | $q_m$ | $R^2$ |
|---|---|---|---|---|---|---|---|
| Au NP | PVA | 2.999 | 0.537 | 0.017 | 0.681 | 1.860 | 0.934 |
| | PVA/gluten (2.5 wt %) | 1.716 | 0.034 | 0.020 | 0.732 | 28.710 | 0.975 |
| | PVA/gluten (5 wt %) | 1.544 | 0.037 | 0.017 | 0.712 | 36.549 | 0.991 |
| Ag NP | PVA | 7.807 | 0.199 | 0.025 | 0.434 | 5.017 | 0.978 |
| | PVA/gluten (2.5 wt %) | 0.659 | 0.036 | 0.054 | 0.399 | 27.700 | 0.996 |
| | PVA/gluten (5 wt %) | 1.665 | 0.031 | 0.188 | 0.531 | 31.847 | 0.995 |

Table 2. Freundlich Isotherm Model Constants and Correlation Coefficients for Adsorption of Two Different Nanoparticles

| | samples | slope ($1/n$) | intercept ($\ln K_f$) | $K_f$ | $R^2$ |
|---|---|---|---|---|---|
| Au NP | PVA | 0.25 | −0.77 | 0.424 | 0.947 |
| | PVA/gluten (2.5 wt %) | 0.62 | 0.35 | 1.42 | 0.97 |
| | PVA/gluten (5 wt %) | 0.23 | −0.76 | 0.46 | 0.99 |
| Ag NP | PVA | 0.65 | −3.11 | 0.04 | 0.95 |
| | PVA/gluten (2.5 wt %) | 0.86 | −0.40 | 0.66 | 0.97 |
| | PVA/gluten (5 wt %) | 0.67 | 0.68 | 1.99 | 0.99 |

Table 3. Pseudo-First-Order and Pseudo-Second-Order Adsorption Rate Constants and Calculated ($Q_e$) and experimental ($Q_e$, exp) at Initial Nanoparticle Concentration of Au NPs and Ag NPs, Respectively

| | | | | pseudo-first-order kinetic model | | pseudo-second-order kinetic model | |
|---|---|---|---|---|---|---|---|
| | sample | time dependent, $Q_e$ (mg/g) (exp) | Langmuir isotherm, $Q_e$ (mg/g) | $Q_e$ (mg/g) | $R^2$ | $Q_e$ (mg/g) | $R^2$ |
| Au NPs | PVA (7 wt %) | 11.2 | 1.86 | 0.60 | 0.83 | 10.03 | 0.95 |
| | PVA/gluten (2.5 wt %) | 17.38 | 28.71 | 1.08 | 0.89 | 16.85 | 0.98 |
| | PVA/gluten (5 wt %) | 23.50 | 36.54 | 1.38 | 0.89 | 23.00 | 0.99 |
| Ag NPs | PVA (7 wt %) | 9.5 | 5.017 | 0.86 | 0.78 | 8.85 | 0.97 |
| | PVA/gluten (2.5 wt %) | 24.61 | 27.70 | 8.98 | 0.82 | 23.98 | 0.99 |
| | PVA/gluten (5 wt %) | 40.25 | 31.84 | 10.08 | 0.87 | 40.78 | 0.99 |

spun hybrid PVA/gluten nanofibers was discussed. The results show that smooth and uniform nanofibers were formed under optimized electrospinning conditions. The PVA/gluten nanofiber mats can be rendered to be water stable via cross-linking and are able to absorb negatively charged nanoparticles through electrostatic interaction. The Langmuir isotherm model gave a better fit than Freundlich as shown by the higher $R^2$ value. The maximum adsorption capacity $Q_e$ varies from 36.54 mg/g and 31.84 mg/g for Au NPs and Ag NPs, respectively, for PVA/gluten in nanofibers (5 wt %). We anticipate that the highly stable hybrid nanofibrous mats with a large number of polar functional groups prepared may be useful in the remediation of negatively charged nanoparticles or other toxic pollutants from contaminated water.

## ■ ASSOCIATED CONTENT

### Supporting Information

TEM images, particle size and distribution, zeta potential, UV spectrum of Au and Ag NPs, and pseudo-first-order and pseudo-second-order kinetic model plots were shown, respectively. This material is available free of charge via the Internet at http://pubs.acs.org.

## ■ AUTHOR INFORMATION

### Corresponding Author

*E-mail: chmsv@nus.edu.sg. Tel.: (65) 65164327. Fax: (65) 67791691.

### Notes

The authors declare no competing financial interest.

## ■ ACKNOWLEDGMENTS

The authors thank the Singapore−Peking−Oxford Research Enterprise (R-143-000-468-112, R-706-000-100-414) and the National University of Singapore (Tier 1) for financial support of the work. R.M., D.S., and R.F.D. also thank the National University of Singapore for a scholarship for graduate studies.

## ■ REFERENCES

(1) Musee, N. Nanowastes and the environment: Potential new waste management paradigm. *Environ. Int.* **2011**, *37*, 112−128.

(2) Oberdorster, G.; Oberdorster, E.; Oberdorster, J. Nanotoxicology: An emerging discipline evolving from studies of ultrafine particles. *Environ. Health Perspect.* **2005**, *113*, 823−839.

(3) Jia, G.; Wang, H. F.; Yang, L.; Wang, X.; Pei, R. J.; Yan, T.; Zhao, Y. L.; Guo, X. B. Cytotoxicity of carbon nanomaterials: Single-wall nanotube, multi-wall nanotube, and fullerene. *Environ. Sci. Technol.* **2005**, *39*, 1378−1383.

(4) Lam, C. W.; James, J. T.; McCluskey, R.; Hunter, R. L. Pulmonary toxicity of single-wall carbon nanotubes in mice 7 and 90 days after intratracheal instillation. *Toxicol. Sci.* **2004**, *77*, 126−134.

(5) Peters, K.; Unger, R. E.; Kirkpatrick, C. J.; Gatti, A. M.; Monari, E. Effects of nano-scaled particles on endothelial cell function in vitro: Studies on viability, proliferation and inflammation. *J. Mater. Sci.: Mater. Med.* **2004**, *15*, 321−325.

(6) Rahman, Q.; Lohani, M.; Dopp, E.; Pemsel, H.; Jonas, L.; Weiss, D. G.; Schiffmann, D. Evidence that ultrafine titanium dioxide induces micronuclei and apoptosis in Syrian hamster embryo fibroblasts. *Environ. Health Perspect.* **2002**, *110*, 797−800.

(7) Smith, L. A.; Ma, P. X. Nano-fibrous scaffolds for tissue engineering. *Colloids Surf., B* **2004**, *39*, 125−131.

(8) He, W.; Ma, Z.; Yong, T.; Teo, W. E.; Ramakrishna, S. Fabrication of collagen-coated biodegradable polymer nanofiber mesh and its potential for endothelial cells growth. *Biomaterials* **2005**, *26*, 7606−7615.

(9) Zhu, X.; Cui, W.; Li, X.; Jin, Y. Electrospun fibrous mats with high porosity as potential scaffolds for skin tissue engineering. *Biomacromolecules* **2008**, *9*, 1795−1801.

(10) Wang, X.; Drew, C.; Lee, S. H.; Senecal, K. J.; Kumar, J.; Samuelson, L. A. Electrospun nanofibrous membranes for highly sensitive optical sensors. *Nano Lett.* **2002**, *2*, 1273−1275.

(11) Drew, C.; Liu, X.; Ziegler, D.; Wang, X.; Bruno, F. F.; Whitten, J.; Samuelson, L. A.; Kumar, J. Metal oxide-coated polymer nanofibers. *Nano Lett.* **2003**, *3*, 143−147.

(12) Ding, B.; Kim, J.; Kimura, E.; Shiratori, S. Layer-by-layer structured films of $TiO_2$ nanoparticles and poly(acrylic acid) on electrospun nanofibres. *Nanotechnology* **2004**, *15*, 913−917.

(13) Bi, Y.; Lu, G. Facile synthesis of platinum nanofiber/nanotube junction structures at room temperature. *Chem. Mater.* **2008**, *20*, 1224−1226.

(14) Sundarrajan, S.; Venkatesan, A.; Ramakrishna, S. Fabrication of nanostructured self-detoxifying nanofiber membranes that contain active polymeric functional groups. *Macromol. Rapid Commun.* **2009**, *30*, 1769−1774.

(15) Yoon, K.; Hsiao, B. S.; Chu, B. Functional nanofibers for environmental applications. *J. Mater. Chem.* **2008**, *18*, 5326−5334.
(16) Ma, M.; Hill, R. M.; Lowery, J. L.; Fridrikh, S. V.; Rutledge, G. C. Electrospun poly(styrene-*block*-dimethylsiloxane) block copolymer fibers exhibiting superhydrophobicity. *Langmuir* **2005**, *21*, 5549−5554.
(17) Ma, M.; Gupta, M.; Li, Z.; Zhai, L.; Gleason, K. K.; Cohen, R. E.; Rubner, M. F.; Rutledge, G. C. Decorated electrospun fibers exhibiting superhydrophobicity. *Adv. Mater.* **2007**, *19*, 255−259.
(18) Haider, S.; Park, S. Y. Preparation of the electrospun chitosan nanofibers and their applications to the adsorption of Cu(II) and Pb(II) ions from an aqueous solution. *J. Membr. Sci.* **2009**, *328*, 90−96.
(19) Xiao, S.; Shen, M.; Guo, R.; Wang, S.; Shi, X. Immobilization of zerovalent iron nanoparticles into electrospun polymer nanofibers: Synthesis, characterization, and potential environmental applications. *J. Phys. Chem. C* **2009**, *113*, 18062−18068.
(20) Mahanta, N.; Valiyaveettil, S. Surface modified electrospun poly(vinyl alcohol) membranes for extracting nanoparticles from water. *Nanoscale* **2011**, *3*, 4625−4631.
(21) Mahanta, N.; Leong, W. Y.; Valiyaveettil, S. Isolation and characterization of cellulose-based nanofibers for nanoparticle extraction from an aqueous environment. *J. Mater. Chem.* **2012**, *22*, 1985−1993.
(22) Antonio, R. C.; Eunice, F. S. V.; Glaucia, S. V.; Luis, E. A. Aggregation and adsorption of reactive dyes in the presence of an anionic surfactant on mesoporous aminopropyl silica. *J. Colloid Interface Sci.* **2007**, *309*, 402−411.
(23) Wang, S.; Boyjoo, Y.; Choueib, A. Removal of dyes from aqueous solution using fly ash and red mud. *Water Res.* **2005**, *39*, 129−138.
(24) Woerdeman, D. L.; Ye, P.; Shenoy, S.; Parnas, R. S.; Wnek, G. E.; Trofimova, O. Electrospun fibers from wheat protein: Investigation of the interplay between molecular structure and the fluid dynamics of the electrospinning process. *Biomacromolecules* **2005**, *6*, 707−712.
(25) Zhang, X.; Gozukara, Y.; Sangwan, P.; Gao, D.; Bateman, S. Biodegradation of chemically modified wheat gluten-based natural polymer materials. *Polym. Degrad. Stab.* **2010**, *95*, 2309−2317.
(26) Domeneck, S.; Brendel, L.; Morel, M. H.; Guilbert, S. Swelling behavior and structural characteristics of wheat gluten polypeptide films. *Biomacromolecules* **2004**, *5*, 1002−1008.
(27) Lefebvre, J.; Popineau, Y.; Deshayes, G.; Lavenant, L. Temperature-induced changes in the dynamic rheological behavior and size distribution of polymeric proteins for glutens from wheat near-isogenic lines differing in HMW glutenin subunit composition. *Cereal Chem.* **2000**, *77* (2), 193−201.
(28) Guerrini, L. M.; Oliveira, M. P.; Branciforti, M. C.; Custodio, T. A.; Bretas, R. E. S. Thermal and structural characterization of nanofibers of poly(vinyl alcohol) produced by electrospinning. *J. Appl. Polym. Sci.* **2009**, *112*, 1680−1687.
(29) Li, J. K.; Wang, N.; Wu, X. S. Poly(vinyl alcohol) nanoparticles prepared by freezing-thawing process for protein/peptide drug delivery. *J. Controlled Release* **1998**, *56*, 117−126.
(30) AshaRani, P. V.; Mun, G. L. K.; Hande, M. P.; Valiyaveettil, S. Cytotoxicity and genotoxicity of silver nanoparticles in human cells. *ACS Nano* **2009**, *3*, 279−290.
(31) Samarghandi, M. R.; Zarrabi, M.; Sepehr, M. N.; Amrane, A.; Safari, G. H.; Bashiri, S. Application of acidic treated pumice as an adsorbent for the removal of azo dye from aqueous solutions: kinetic, equilibrium and thermodynamic studies. *Iran. J. Environ. Health Sci. Eng.* **2012**, *9* (1), 9.
(32) Freundlich, H. M. F. Over the adsorption in solution. *Phys. Chem.* **1906**, *57*, 385−470.
(33) Langmuir, I. The adsorption of gases on plane surfaces of glass, mica and platinum. *J. Am. Chem. Soc.* **1918**, *40*, 1361−1403.
(34) Sen, T. K.; Afroze, S.; Ang, H. M. Equilibrium, kinetics and mechanism of removal of methylene blue from aqueous solution by adsorption onto pine cone biomass of pinus radiate. *Water, Air, Soil Pollut.* **2011**, *218*, 499−515.
(35) Mohammad, M.; Maitra, S.; Ahmad, N.; Bustam, A.; Sen, T. K.; Dutta, B. K. Metal ion removal from aqueous solution using physic seed hull. *J. Hazard. Mater.* **2010**, *179*, 363−372.
(36) Vimonses, V.; Lei, S.; Jin, B.; Chow, C. W. K.; Saint, C. Kinetic study and equilibrium isotherm analysis of congo red adsorption by clay materials. *Chem. Eng. J.* **2009**, *148*, 354−364.
(37) Praptowidodo, V. S. Influence of swelling on water transport through PVA-based membrane. *J. Mol. Struct.* **2005**, *739*, 207−212.
(38) Brasch, U.; Burchard, W. Preparation and solution properties of microhydrogels from poly(vinyl alcohol). *Macromol. Chem. Phys.* **1996**, *197*, 223−235.
(39) Zhong, N.; Yuan, Q. Preparation and properties of molded blends of wheat gluten and cationic water-borne polyurethanes. *J. Appl. Polym. Sci.* **2013**, 460−469.
(40) Giles, C. H.; Hassan, A. S. A. Adsorption at organic surfaces V: A study of the adsorption of dyes and other organic solutes by cellulose and chitin. *J. Soc. Dyers Col.* **1958**, *74*, 846−857.
(41) El Badawy, A. M.; Luxton, T. P.; Silva, R. G.; Scheckel, K. G.; Suidan, M. T.; Tolaymat, T. M. Impact of environmental conditions (pH, ionic strength, and electrolyte type) on the surface charge and aggregation of silver nanoparticles suspensions. *Environ. Sci. Technol.* **2010**, *44* (4), 1260−1266.
(42) Hall, K. R.; Eagleton, L. C.; Acrivos, A.; Vermeule, T. Pore- and solid-diffusion kinetics in fixed-bed adsorption under constant-pattern conditions. *Ind. Eng. Chem. Fund.* **1966**, *5* (2), 212−219.
(43) Arias, F.; Sen, T. K. Removal of zinc metal ion ($Zn^{2+}$) from its aqueous solution by kaolin clay mineral: A kinetic and equilibrium study. *Colloids Surf., A* **2009**, *348*, 100−108.